ADVANCED MATERIALS
www.advmat.de

Self-Powered Wearable Electronics Based on Moisture Enabled Electricity Generation

Daozhi Shen, Ming Xiao, Guisheng Zou, Lei Liu, Walter W. Duley, and Y. Norman Zhou**

Most state-of-the-art electronic wearable sensors are powered by batteries that require regular charging and eventual replacement, which would cause environmental issues and complex management problems. Here, a device concept is reported that can break this paradigm in ambient moisture monitoring—a new class of simple sensors themselves can generate moisture-dependent voltage that can be used to determine the ambient humidity level directly. It is demonstrated that a moisture-driven electrical generator, based on the diffusive flow of water in titanium dioxide (TiO_2) nanowire networks, can yield an output power density of up to 4 μW cm^{-2} when exposed to a highly moist environment. This performance is two orders of magnitude better than that reported for carbon-black generators. The output voltage is strongly dependent on humidity of ambient environment. As a big breakthrough, this new type of device is successfully used as self-powered wearable human-breathing monitors and touch pads, which is not achievable by any existing moisture-induced-electricity technology. The availability of high-output self-powered electrical generators will facilitate the design and application of a wide range of new innovative flexible electronic devices.

Wearable and flexible electronics, including smart mobile devices and microelectrochemical systems (MEMS), have been booming recently and hold a great promise in the next generation electronics. However, most of them are powered by batteries that require regular charging and eventual replacement, which would cause environmental issues and complex management problems. To satisfy this requirement, a series of advanced energy-generation technologies based on triboelectric,[1–3] piezoelectric,[4,5] and thermoelectric[6–8] effects are being developed to harvest clean energy directly from environment. Very recently, water vapor or moisture, a vast kind of resource existing ubiquitously on earth and in biological organisms, has been initiatively exploited as a novel harvestable energy to generate electricity.[9,10] Very different from previous energy harvesting technologies, this initialization expands the range of natural phenomena that can be used to generate electric power.

In this context, the appearance of a constant voltage associated with evaporation-induced water flow in porous carbon has been reported in a previous study,[11] but the output power density is low and physical/chemical mechanisms responsible for this effect are still uncertain. The diffusion of moisture has also been shown to generate electricity from graphene oxide, but prepolarization under a constant electric field is needed.[9,12] Meanwhile, these moisture enabled generators have not been initially demonstrated to have availability to be flexible and further to be used as self-powered wearable devices. There is then an urgent need for the development of mechanically flexible, high-output-power electrical generators using energy extracted from ambient water-vapor/moisture and making them applicable in self-powered wearable electronics.

Herein, we report the prototype of a new device that eliminates the need for external power sources in the detection of moisture related behavior. The construction is based on a new energy harvesting device involving the direct generation of electrical power from ambient moisture. This device has strongly hydrophilic titanium dioxide (TiO_2) nanowire networks (TDNNs) containing 3D nanochannels, which facilitate the diffusion of water molecules accreted from ambient moisture. The resulting moisture-enabled electricity generator (MEEG) can generate an open-circuit voltage of up to ≈0.5 V combined with a power density of ≈4 μW cm^{-2}. These output characteristics are superior (by two orders of magnitude) to those of carbon-black generators. The moisture in human breath is capable of generating enough electricity to power a commercial light-emitting diode (LED). The output power from a TDNN MEEG has also been used to charge a capacitor of the type utilized in high power applications. Significantly, TDNN MEEGs, in contrast to other moisture enabled nanogenerators, are intrinsically flexible and

D. Shen, Prof. G. Zou, Prof. L. Liu
State Key Laboratory of Tribology
Tsinghua University
Beijing 100084, P. R. China
E-mail: liulei@tsinghua.edu.cn
D. Shen, Prof. W. W. Duley
Department of Physics and Astronomy
University of Waterloo
Waterloo, Ontario N2L 3G1, Canada
D. Shen, M. Xiao, Prof. Y. N. Zhou
Waterloo Institute of Nanotechnology
University of Waterloo
Waterloo, Ontario N2L 3G1, Canada
E-mail: nzhou@uwaterloo.ca
D. Shen, M. Xiao, Prof. Y. N. Zhou
Centre for Advanced Materials Joining
University of Waterloo
Waterloo, Ontario N2L 3G1, Canada

DOI: 10.1002/adma.201705925

maintain their output characteristics after 10 000 bending cycles. This new type of device is successfully used as self-powered wearable human-breathing monitors and touch pads. The availability of such generator facilitates the design of a wide range of self-powered flexible electronics and holds a promise in the creation of a new range of innovative electronic devices.

The experimental configuration for measuring the electrical characteristics of the TDNN MEEG is illustrated in **Figure 1**a. Electrophoretic deposition was used to uniformly deposit TiO_2 nanowires on a highly flexible poly(ethylene terephthalate) substrate coated with indium tin oxide (ITO) (Figures S1 and S2, Supporting Information). The charged nanowires suspended in the colloidal solution migrate toward the substrate under a 30 V bias. Applying this bias for 1 min forms a homogeneous network of nanowires containing an abundance of interstitial nanochannels (Figure 1b). The thickness of the TDNN can be readily controlled by the applied voltage or by varying the deposition time (Figure S3, Supporting Information). Following deposition, the substrate was coated with a uniform layer of TDNN and then annealed at 100 °C for 12 h to improve the adhesion between the network and the substrate. An aluminum (Al) pattern with a thickness of 100 nm was then deposited as a top electrode on the surface of the network using electron beam evaporation. The final 1.2 × 1.2 cm flexible device is shown in Figure 1c.

Scanning electron microscopy (SEM) (Figure 1d,f) shows that the final TDNN has thickness of ≈10 µm and consists of loosely aggregated nanowires each with a diameter of ≈100 nm. The nanochannels between these nanowires are <100 nm wide and permit moisture to diffuse into the network (in Figure 1e; Figures S4 and S5, Supporting Information). The capillary nanostructure of these networks facilitates the permeation and diffusion of water, which results in the contact angle of 5°–10° as shown in Figure S6 (Supporting Information). A high-resolution transmission electron microscopy image (inset in Figure 1f) shows that as-prepared nanowires have a lattice spacing of 0.47 nm, corresponding to the (002) plane of anatase TiO_2.[13] The selected area electron diffraction pattern as shown in Figure S7 (Supporting Information) confirms this phase structure.

To evaluate the response of the TDNN device to environmental moisture, the unit was placed in a chamber with controlled relative humidity (RH) (Figures S8 and S9, Supporting Information). It was found that the resistance of the TDNN device is a strong function of humidity and decreases as the RH increases (Figure S10, Supporting Information). With RH set at

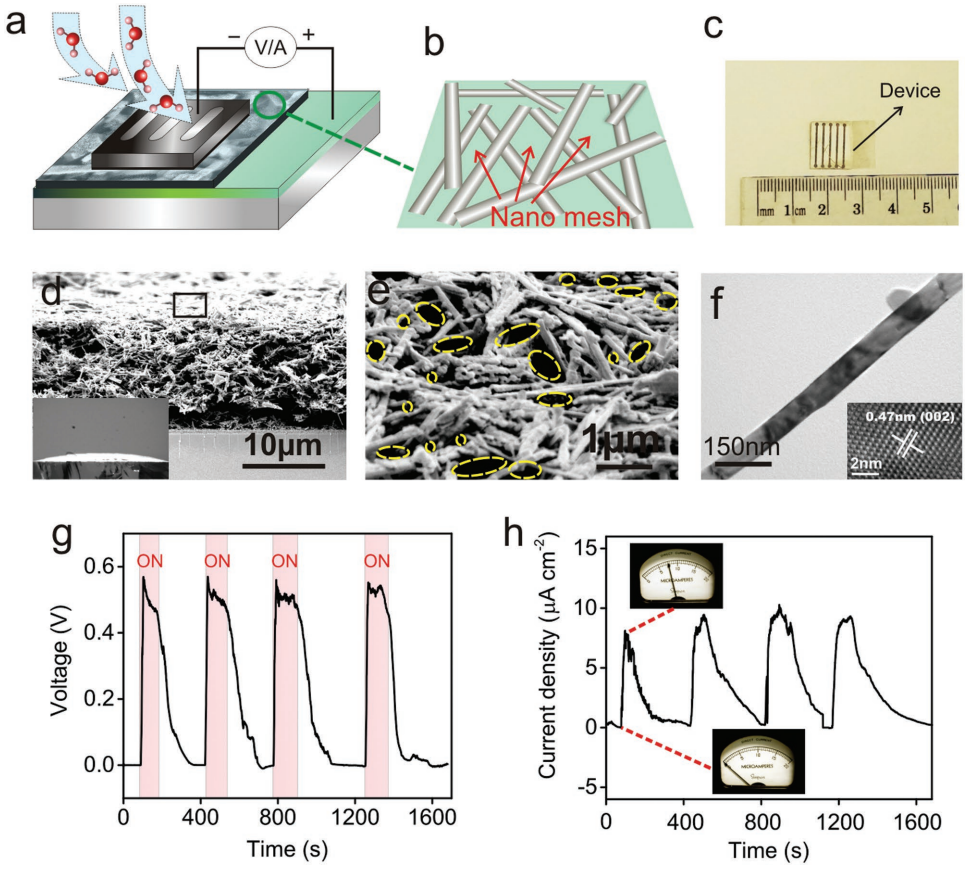

Figure 1. Device fabrication and characterization. a) Device schematic and configuration used for electrical measurements. b) A schematic representation of the resulting nanomesh structure in a TDNN. c) Photograph of an MEEG against a centimeter ruler. d) SEM image of the cross-section of a TDNN. Inset: wetting condition of TDNN. e) Magnified SEM image of the TDNN as marked in (d). Some pores are identified. f) Transmission electron microscopy (TEM) of a single nanowire. Inset: high-resolution TEM (HRTEM) image. g) Open-circuit voltage and h) short-circuit current density in response to an increase in RH to 85%. RH is increased during the times indicated by the shaded areas in g). The insets in (h) show the deflection of a microammeter connected across the output terminals of the MEEG during the RH cycles shown in (g).

85%, the open-circuit voltage (V_{oc}) of the TDNN MEEG rises to ≈0.52 V over a 10 s time interval (Figure 1g) and the short-circuit current density (I_{oc}) approaches ≈8 µA cm^{-2} (Figure 1h). No electricity generated from the device when only pure nitrogen flows into the chamber (Figure S11, Supporting Information). The measured output power density (≈4.16 µW cm^{-2}) then exceeds that reported for fluidic-electric generators, i.e., three orders of magnitude better than that of monolayer graphene (3.5 nW cm^{-2})[14] or polypyrrole (0.7 nW cm^{-2})[15] generators, and two orders of magnitude better than that of carbon-black generators (40 nW cm^{-2}).[11] Unlike most other moisture-based generators,[1,8,16] the output voltage of the TDNN MEEG is asymmetric and has constant polarity. This self-rectifying property may eliminate the need for a separate rectifier in future applications.

The insets in Figure 1h show the response of a microammeter connected across the device before and after the application of moisture as indicated in Figure 1g. When the RH is reduced to the ambient level, the output voltage and current decreases over a timescale of ≈150 s to that appearing in the device at the ambient humidity. The time constant for the humidity to be lowered to the ambient level is typically ≈150 s (Figure S12, Supporting Information). It can be seen that the output voltage from the TDNN MEEG follows the reduction in humidity over a similar (≈120 s), but not identical timescale. This difference can be attributed to the nonlinear response of the device (**Figure 2**). As shown in Figure 1g, the output voltage and current response are repeatable in each cycle, indicating that the output is reproducible. The temperature of chamber environment is quiet stable

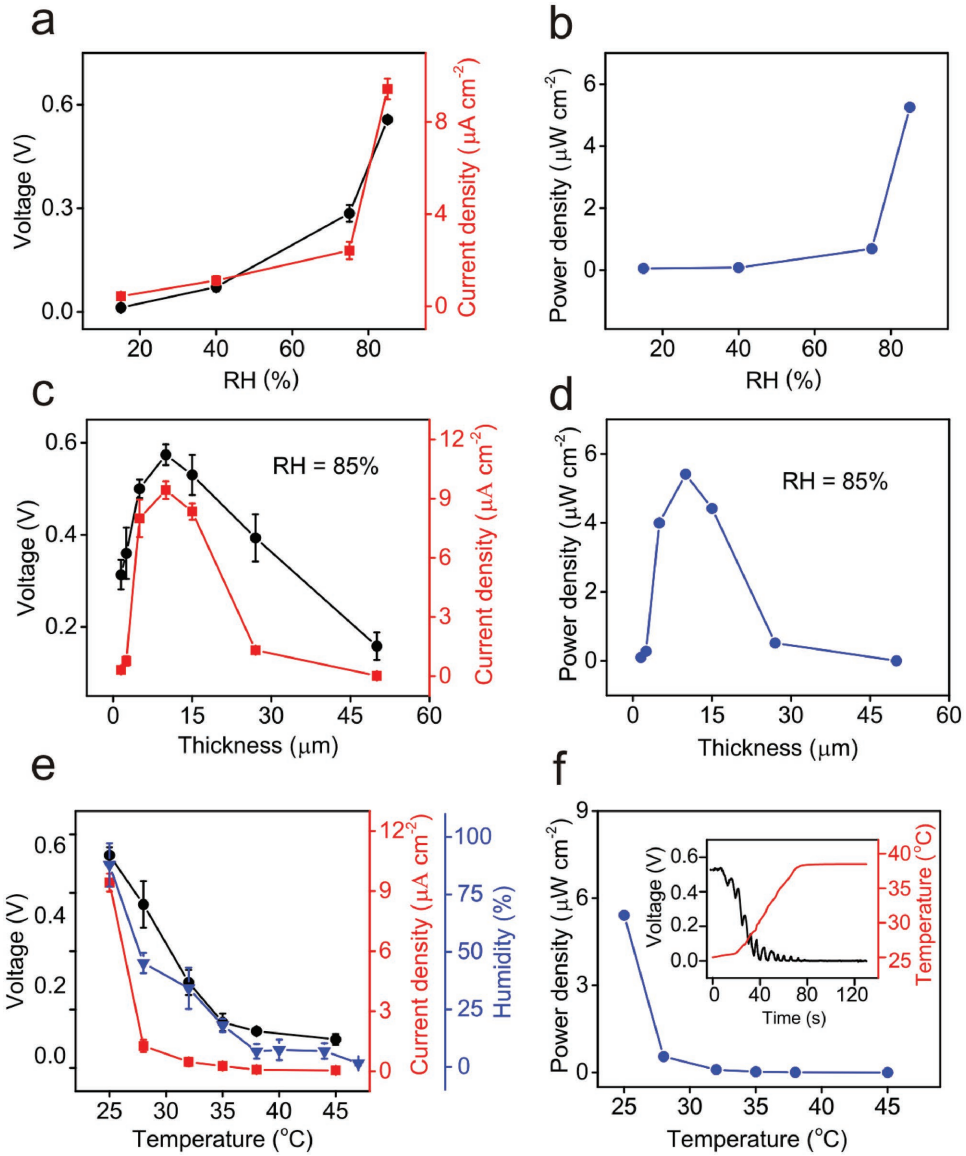

Figure 2. Factors that affect the electrical output of the MEEG. a) Output voltage and short-circuit current density versus RH for a device with a 10 µm thick TDNN layer. b) Power output versus RH with a TDNN thickness of 10 µm. c) Output voltage and current density versus TDNN thickness. d) Power output versus thickness at an RH = 85%. e) Output voltage and current density at different temperatures. The corresponding RH is also shown. f) Power density at different temperatures. The inset shows how output voltage changes with time during an increase in temperature.

(24.3 ± 0.3 °C) in a period of 10 min (Figure S13, Supporting Information), but the humidity level vibrates easily due to the difficulties in humidity control each time. Thus, fluctuations in the electricity response can be attributed to variation of humidity level in a series of cycles (Figure S14, Supporting Information). Some other factors, such as mechanical vibration, may also contribute to these fluctuations.

The effect of changing the RH, network thickness, and ambient temperature on the performance of TDNN MEEGs is summarized in Figure 2. As the electrical output derives from the interaction between moisture and TiO_2 nanowires, the RH in the environment can play a key role in the performance of the device. As shown in Figure 2a, the output voltage and current along with output power increase with RH (Figure 2b), indicating that there is a strong correlation between the electrical generating capacity of the TDNN MEEG and moisture content. The nonlinear relationship between voltage (or current) and RH may be attributed to that the percentage of ions in a fixed amount of water increases with RH (see Figure S15, Supporting Information). Both the output voltage and the current exhibit a nonlinear dependence on the thickness of the TDNN layer. The output power density initially increases with the thickness of the TDNN until the thickness reaches ≈10 µm. The output power density subsequently decreases with a further increase in thickness (Figure 2c,d). Observation of a peak in output power density at a thickness of ≈10 µm shows that the electrical response is related to the diffusion length for water molecules in the nanowire network. When the TDNN is too thin, the gradient in ion concentration is small and the output diminishes. When the TDNN is too thick, the diffusion pathway for water molecules and ions in the internal nanochannels is too long, preventing diffusive flow to the bottom electrode. The effects of temperature are summarized in Figure 2e and show that both the output voltage and power density decrease rapidly as the temperature increases above 25 °C. In addition, the output voltage measured at ≈7 s between high RH conditions after termination of the high RH state (Figure 1g) decreases rapidly with an increase in temperature above 25 °C (see inset in Figure 2f). These properties can be attributed to a reduction in RH as the temperature is increased leading to a decrease in output voltage (Figure 2a). The electrical generation properties of deposits consisting of vertical TiO_2 nanorods (Figure S6d, Supporting Information) have also been measured at the same RH as in loosely aggregated samples. These vertical nanorod arrays have a higher spatial density with fewer channels for diffusion. Such surfaces also exhibit reduced wettability (Figure S6c, Supporting Information). As a result, the output voltage is only 30 mV (i.e., >16 times smaller than in TDNNs) (Figure S16, Supporting Information). A range of different conductive materials have been evaluated as bottom and top electrodes in TDNN MEEG devices. We find that devices fabricated with these electrodes are all capable of generating output voltages in the ≈0.25–0.30 V range at an RH of ≈70% (**Figure 3**a). The configuration of TDNN sandwiched with similar metals such as Al-TDNN-Al and ITO-TDNN-ITO can also yield a comparable voltage under moisture environment, indicating electrochemical reaction due to work function difference electrodes may play a minor role in voltage generation (Figures S17 and 18, Supporting Information). It is significant that a structure with gold as electrodes is found to produce an output voltage of ≈0.3 V as this indicates that the generation of electrical power originates from the interaction between water molecules and the surface of TiO_2 nanowires as gold is inert with respect to water and TiO_2. As expected, virtually no voltage is generated

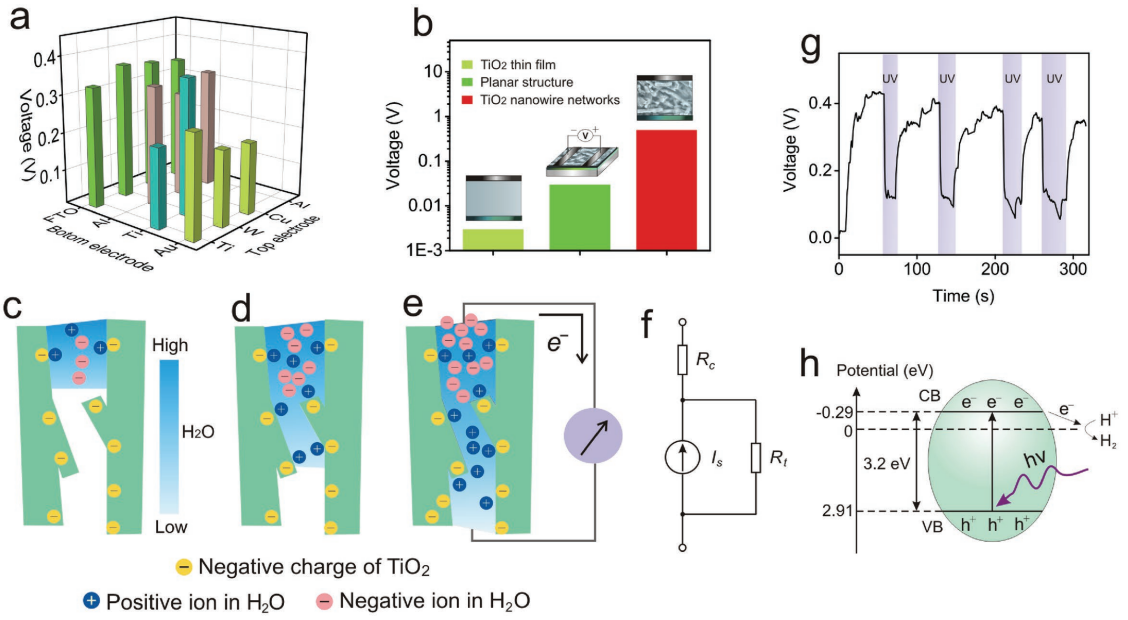

Figure 3. Operational mechanism of the MEEG. a) Output voltage of MEEGs using different electrode materials. b) Comparison of output voltage of various TiO_2 based MEEGs structures. c–e) Postulated mechanism of ion diffusion along the negatively charged walls of a TiO_2 nanochannel. f) Equivalent electrical circuit of an MEEG. I_s, R_t, and R_s represent the current, internal resistance and contact resistance of the TiO_2 and electrode, respectively. g) Irradiation with UV light reduces the output voltage. h) Photoexcitation process. UV light excites electrons from the valence band (VB) to the conduction band (CB). Excited electrons migrate to the surface of the nanowire where they combine with H^+ in the electrical double layer generating H_2.

from the present electrode configuration when TiO_2 is removed (Figure S19, Supporting Information). The effect of different structures on the open-circuit output of the TDNN MEEG is summarized in Figure 3b. It is apparent that only the sandwiched TDNN configuration results in significant power generation when exposed to moisture. This can be attributed to the fact that only the TDNN configuration facilitates the diffusion of water molecules deep into the network. It also indicates that the voltage is generated because of a gradient in the concentration of water molecules along the nanochannels from the top to the bottom electrodes. Little output voltage appears across the electrodes when the TDNN is applied in planar form as the water concentration is similar at all locations on the surface.

The above results clearly show that the electrical generating capacity of TDNN MEEGs arises from the diffusion of water molecules along the many nanochannels that exist in the nanowire network. The streaming potential,[17–19]a classic electrokinetic phenomenon induced by driving ionic solutions through narrow channels under a pressure gradient, is likely the source of the voltage measured across the electrodes. As synthesized, TiO_2 nanowires are negative charged[20,21] in neutral water and have a zeta potential of ≈−20 mV (Figure S20, Supporting Information). Nanochannels inside a loosely aggregated nanowire network are heteromorphic and range in diameter to <100 nm (Figure S4, Supporting Information). The putative mechanism for the generation of electrical power can then be simplified as shown schematically in Figure 3c–e. During the diffusion of water down a nanochannel, positive ions (primarily H^+) in the water are attracted toward the TiO_2 surface due to the negative surface charge on TiO_2. These then form an electrical double layer (DL) extending several nanometers out from the surface. As water molecules diffuse into the narrowest channels having widths that are of similar size to that of the DL, the flow of negative ions is impeded[22,23] and only the smaller positive ions can pass deeper into the channel as shown in Figure 3d. Capillary flow then produces a separation of negative and positive ions and the resulting charge imbalance then establishes an electric field along the channel from the bottom to the top electrode. Current flow in an external circuit is as shown in Figure 3e and is confirmed by the microammeter in Figure 1a,g. The output voltage has opposite polarity in structures comprised of aggregated ZnO nanoparticles where the zeta potential is ≈+25 mV (Table S1, Supporting Information).

This mechanism is also supported by the observed decrease in output voltage when the MEEG is irradiated with ultraviolet (UV) light (Figure 3g) as UV radiation transfers electrons into the conduction band where they migrate to the surface and react with protons (Figure 3h).[24,25] This reaction decreases the gradient in charge density that gives rise to the electric field established by the diffusion of protons. It is significant that no change in output voltage is found on irradiation with sunlight (Figure S21, Supporting Information), indicating that only photons with energies greater than the bandgap energy in TiO_2 (anatase) are effective.

According to the theory of nanofluids, the electrical streaming current generated by a conventional ionic charge cloud adjacent to the walls of a channel is[26]

$$I_s = -\frac{\varepsilon\varepsilon_0\zeta wh\Delta P}{\eta L} \quad (1)$$

where ε_0 is the permittivity of free space, ε is the relative permittivity of the fluid, ζ is the zeta potential at the shear plane of the channel wall, w is the width, and h is the height of the wall, ΔP is the pressure difference between the ends of the channel, η is the fluid viscosity, and L is the length of the channel. From our measurements, increasing the thickness of the TDNN increases L resulting in a lower electrical output as shown in Figure 2c,d. As RH becomes larger the driving force for water diffusion, and hence ΔP, increases, resulting in a higher output power as shown in Figure 2a,b. With a streaming current arising from ionic diffusion, the equivalent electrical circuit for voltage generation can be represented as a current source I_s having an internal resistance R_t (Figure 3f). R_c in this circuit represents the contact resistance between the electrodes and the TDNN active medium.

To increase the output, MEEG cells can be connected in series or in parallel as shown in the insets in **Figure 4**a,b, respectively. The outputs of these test circuits are labeled with the number of individual cells. Individual cells generate an output voltage of ≈0.5 V while a series combination of two and three cells results in ≈0.9 and ≈1.3 V, respectively. Similarly, three cells connected in parallel increases the short-circuit current from ≈8 to ≈25 μA. As the output current depends on the contact area between the TDNN and the top electrode, the output can be further increased by optimizing this geometry to incorporate a porous structure. The output can also be enhanced by stacking MEEG cells in a 3D configuration.

As the framework of the TDNN MEEG is nonrigid, the generator can be used in applications where flexibility is required. To assess this capability, mechanical bending tests were carried out as shown in Figure 4c. The data indicate that the output voltage remains approximately constant after 10 000 cycles at a bending radius of 6 mm. A similar result was obtained at bending radii ranging from 0.3 to 40 mm (Figure S22, Supporting Information). Small changes in output voltage during these tests can be attributed to fluctuations in ambient temperature and humidity. We believe that this is the first report of a mechanically flexible MEEG generator and suggests that these devices may have wide application in portable electronics. To explore one of these possible applications, we have investigated if this device can be powered by the moisture present in human breath. Figure 4d shows that the generator produces an output of ≈0.25 V under resting conditions. After exertion by jogging for 10 min, the output voltage rises to ≈0.4 V. This effect can be attributed to the increased humidity in exhaled breath after exercise. In another test, six TDNN MEEG cells were connected in series and used to power an LED using the moisture from human breath (Figure 4e,f). Under these conditions, the output of the LED is bright enough to be seen in daylight (see Movie S1, Supporting Information).

Although the output power density of the TDNN MEEG reported here surpasses that obtainable from most other nanogenerators, and is sufficient to drive low-power micro/nanoelectronics, the output is still too low to directly power most conventional electronic devices. To solve this problem, we find that the MEEG can be used to charge a bank of capacitors as shown in Figure 4g and Figure S23 (Supporting Information). For example, six capacitors connected in parallel can be directly charged to ≈0.5 V using a single MEEG. These capacitors were

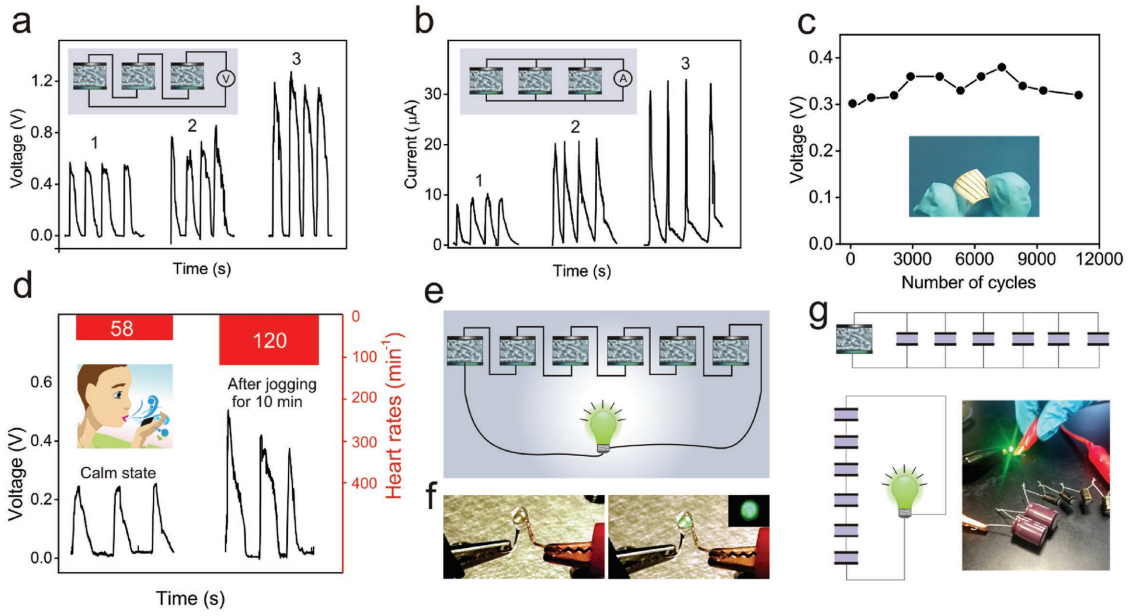

Figure 4. Applications of the MEEG in powering commercial LED and flexibility test. a) Output voltage from one, two and three MEEGs connected in series. RH = 85%. b) Short-circuit current from one, two, and three MEEG generators connected in parallel. RH = 85%. c) Output voltage during a bending test extending over 11 000 cycles. d) Voltage output of a TDNN MEEG in response to the moisture from mouth in human breath. e) Commercial LED running on electricity from six MEEGs connected in series. f) As above in off/on condition. Inset: LED in dark room. g) Simultaneous charging of six capacitors (each with 100 μF) with a single TDNN MEEG. The capacitors are then connected in series to power a commercial LED.

then connected in series, producing an output voltage of 3.0 V. The energy stored in this capacitor bank was then used to power an LED (Figure 4g).

Since the electrical response of a TDNN MEEG is strongly dependent on humidity, MEEGs are promising for applications involving the detection of humidity levels in free-standing systems in the absence of an external power supply. For example, it is known that human-breathing characteristics (e.g., breath frequency, depth, and intensity), are symptomatic of physiological conditions such as anxiety,[27] asphyxia,[28] epilepsy,[29] and incipient heart attack.[30] Dynamic breathing characteristics under several different conditions, as detected by a self-powered wearable MEEG, are shown in **Figure 5**. Figure 5a and Figure S24 (Supporting Information) show that a flexible MEEG located 0.8 cm from the human nose produces voltage pulses with amplitude ≈20 mV in response to the moisture in human breath under normal breathing conditions. The repetition frequency of these voltage pulses coincides with the breathing rate (20 breaths min^{-1}). A similar result, with well separated voltage pulses, is obtained when the breathing rate is increased to 38 breaths min^{-1} (Figure 5d). It is apparent that an increase in breathing rate is accompanied by an increase in the amplitude of the output signal while a reduction in this rate reduces the output signal (Figure 5c,d). This implies that the RH in each breath is enhanced when the breathing rate is increased. A rapid response to different breathing conditions is successfully obtained for applications of MEEG technology in self-powered wearable detectors used for monitoring of human physiology via detection of breathing conditions.

A wearable self-powered touch pad based on TDDN MEEG technology for sensing human fingers has also been constructed as shown in Figure 5e–h. No external power is required. The flexible MEEG produces voltage pulses with amplitude of ≈150 mV in response to the moisture released from the human finger during contact. As found for the breath monitor, the touch sensor incorporating an MEEG exhibits a rapid response even when the rate of touching reaches 35 touches min^{-1} (see Figure 5e,f). As the voltage generated is a strong function of the pressure exerted during contact, the amplitude of each pulse is somewhat variable (Figure 5g). This suggests that the response is proportional to both moisture and mechanical force enabling a new type of detection mode. The response of another device with a touch pad consisting of a 3 × 3 grid structure is shown in Figure 5g. The width of each bar in this device was 0.5 mm. Each self-powered sensor unit can produce a voltage of ≈150 mV when contacted with a finger. This example of a possible application of a moisture enabled generator shows promise for the development of self-powered touch panels and artificial skins for consumer electronics and flexible robotic applications. It should be noted that the voltage generation of MEEG is easily affected by the ambient parameters during wearable application (Figure 2). The amplitude of voltage pulses generated from both breathing monitor and touch panel decreases with the increase of device temperature (Figures S25 and S26, Supporting Information). However, the voltage pulses can still be easily separated if the devices work in a proper range of temperatures (<35 °C for breathing monitor and <32 °C for touch panel). These devices may be more suitable in some cases where ambient parameters are well controlled, setting intensive care unit for example. We believe the application can be further extended by some optimizations of the device structures as well as practical integration, which needs intensively investigated in the future.

In summary, we have developed a new type of electrical generator (MEEG) based on a TDNN sandwich structure. This

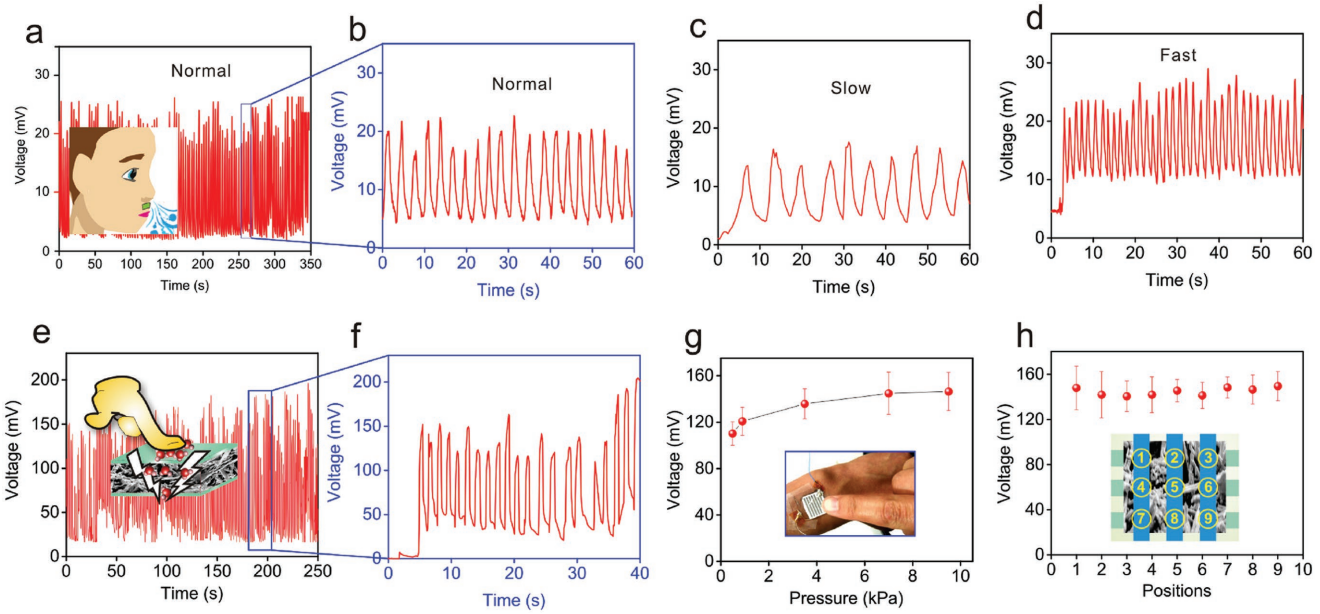

Figure 5. a–h) Applications of TDNN MEEG in self-powered wearable breath monitors (a–d) and touch panels (e–h). a) Output voltage at a distance of 0.8 cm from the nose. Breathing occurred in a "calm state" condition. Inset: A schematic of the MEEG configuration during the test. b) Expanded signal extracted from the plot as marked in (a). c,d) MEEG output voltage during slow breathing (c) and fast breathing (d). e) Output voltage during touching with a human finger. Inset: A schematic of the voltage generation in the self-powered touch sensor. f) Expanded signal extracted from the plot as marked in (e). g) Output voltage of a touch sensor versus touch pressure. Inset: A finger touching the self-powered sensor worn on the wrist. h) Output voltage from a distribution of touch pad sensors on a 3 × 3 grid cross-bar structure during touching with a human finger.

device is shown to efficiently harvest energy directly from moisture, including that presents in human breath. Electricity is generated from the diffusion of ions through the many 3D nanochannels in the TDNN. At a relative humidity of 85%, the output power density exceeds ≈4 μW cm^{-2} from a 1.2 × 1.2 cm device, which is three orders of magnitude better than that from monolayer graphene or polypyrrole generators. The electrical output can be further enhanced by optimization of the top electrode geometry and by integration of MEEG cells into a 3D assembly. An array of TDNN MEEGs has been used to power a commercial LED using the moisture in human breath. The illuminated LED is bright enough to be clearly seen in daylight. We demonstrate that the output of moisture-powered MEEGs can also be used to charge capacitors for devices requiring high power. Significantly, TDNN MEEGs are mechanically flexible, making them unique among moisture enabled electricity generators. As the first demonstration of practical applications in self-powered wearable electronics, this new type of device is successfully used as self-powered wearable human-breathing monitors and touch pads. This combination of properties suggests that TDNN MEEGs are promising structures for harvesting energy from biological systems and facilitate the design of a wide range of self-powered flexible electronics and holds a promise in the creation of a new range of innovative electronic devices.

Experimental Section

A detailed description of procedures and characterization methods are available in the Supporting Information.

Supporting Information

Supporting Information is available from the Wiley Online Library or from the author.

Acknowledgements

D.S and M.X. contributed equally to this work. This work was supported by the National Key Research and Developing Program (Grant No. 2017YFB1104900), the National Natural Science Foundation of China (Grant Nos. 51520105007 and 51775299), and the Natural Science and Engineering Research Council (NSERC) of Canada. D.S. greatly acknowledges the China Scholarship Council (CSC) for the graduate fellowship.

Conflict of Interest

The authors declare no conflict of interest.

Keywords

fluidic electricity, moisture, nanogenerators, self-powered sensors

Received: October 11, 2017
Revised: December 20, 2017
Published online: March 24, 2018

[1] G. Zhu, J. Chen, T. Zhang, Q. Jing, Z. L. Wang, *Nat. Commun.* **2014**, *5*, 3426.
[2] S. Wang, L. Lin, Z. L. Wang, *Nano Lett.* **2012**, *12*, 6339.

[3] J. Chen, G. Zhu, W. Yang, Q. Jing, P. Bai, Y. Yang, T.-C. Hou, Z. L. Wang, *Adv. Mater.* **2013**, *25*, 6094.
[4] H. Fu, R. E. Cohen, *Nature* **2010**, *403*, 281.
[5] H. Maiwa, N. Lizawa, D. Togawa, T. Hayashi, *Appl. Phys. Lett.* **2013**, *82*, 1760.
[6] C. J. Vineis, A. Shakouri, A. Majumdar, *Adv. Mater.* **2010**, *22*, 3970.
[7] I. Chowdhury, R. Prasher, K. Lofgreen, G. Chrysler, *Nat. Nanotechnol.* **2009**, *4*, 235.
[8] S. Xu, Y. Qin, C. Xu, Y. Wei, R. Yang, Z. L. Wang, *Nat. Nanotechnol.* **2010**, *5*, 366.
[9] F. Zhao, H. Cheng, Z. Zhang, L. Jiang, L. Qu, *Adv. Mater.* **2015**, *27*, 4351.
[10] K. Liu, P. Yang, S. Li, J. Li, T. Ding, G. Xue, Q. Chen, G. Feng, J. Zhou, *Angew. Chem., Int. Ed. Engl.* **2016**, *55*, 8003.
[11] G. Xue, Y. Xu, T. Ding, J. Li, J. Yin, W. Fei, Y. Cao, J. Yu, L. Yuan, L. Gong, J. Chen, S. Deng, J. Zhou, W. Guo, *Nat. Nanotechnol.* **2017**, *12*, 317.
[12] F. Zhao, Y. Liang, H. Cheng, L. Jiang, L. Qu, *Energy Environ. Sci.* **2016**, *9*, 912.
[13] D.-D. Qin, Y.-P. Bi, X.-J. Feng, W. Wang, G. D. Barber, T. Wang, Y.-M. Song, X.-Q. Lu, T. E. Mallouk, *Chem. Mater.* **2015**, *27*, 4180.
[14] J. Yin, X. Li, J. Yu, Z. Zhang, J. Zhou, W. Guo, *Nat. Nanotechnol.* **2014**, *9*, 378.
[15] M. Ma, L. Guo, D. G. Anderson, R. Langer, *Science* **2013**, *339*, 186.
[16] C. J. Hu, Y. H. Lin, C. W. Tang, M. Y. Tsai, W. K. Hsu, H. F. Kuo, *Adv. Mater.* **2011**, *23*, 2941.
[17] C.-C. Chang, R.-J. Yang, M. Wang, J.-J. Miau, V. Lebiga, *Phys. Fluids* **2012**, *24*, 072001.
[18] K. C. Hon, C. Zhao, C. Yang, S. C. Low, *Appl. Phys. Lett.* **2012**, *101*, 143902.
[19] F. H. J. van der Heyden, D. J. Bonthuis, D. Stein, C. Meyer, C. Dekker, *Nano Lett.* **2007**, *7*, 1022.
[20] M. Kosmulski, E. Matijevic, *Colloids Surf.* **1992**, *64*, 57.
[21] R. Sprycha, *J. Colloid Interface Sci.* **1986**, *110*, 278.
[22] R. Karnik, R. Fan, M. Yue, D. Li, P. Yang, A. Majumdar, *Nano Lett.* **2005**, *5*, 943.
[23] L.-H. Yeh, Y. Ma, S. Xue, S. Qian, *Sens. Actuators, B* **2015**, *215*, 266.
[24] S. Y. Tee, K. Y. Win, W. S. Teo, L.-D. Koh, *Adv. Sci.* **2017**, *4*, 1600337.
[25] S. Nick, A. V. Emeline, V. K. Ryabchuk, V. N. Kuznetsov, Y. M. Artemev, S. Horikoshi, *ACS Energy Lett.* **2016**, *1*, 931.
[26] Y. Xie, J. D. Sherwood, L. Shui, A. van den Berg, J. C. T. Eijkel, *Lab Chip* **2011**, *11*, 4006.
[27] F. H. Wilhelm, W. T. Roth, *Biol. Psychol.* **2001**, *57*, 105.
[28] C. Ashley, D. Burton, Y. B. Sverrisdottir, M. Sander, D. K. McKenzie, V. G. Macefield, *J. Physiol.* **2010**, *588*, 701.
[29] G. L. Morris, W. M. Muller, *Neurology* **1999**, *53*, 1731.
[30] R. J. Goldberg, P. G. Steg, I. Sadiq, C. B. Granger, E. A. Jackson, A. Budaj, D. Brieger, A. Avezum, S. Goodman, *Am. J. Cardiol.* **2002**, *89*, 791.

